Langmuir

INVITED FEATURE ARTICLE

pubs.acs.org/Langmuir

Recent Progress with Functional Biosupramolecular Systems

David Alonso Doval, Jetsuda Areephong, Eun-Kyoung Bang, Leonardo Bertone, Pierre Charbonnaz, Andrea Fin, Nai-Ti Lin, Marco Lista, Stefan Matile,* Javier Montenegro, Edvinas Orentas, Naomi Sakai, Duy-Hien Tran, and Andreas Vargas Jentzsch

Department of Organic Chemistry, University of Geneva, Geneva, Switzerland

ABSTRACT: The objective of this account is to summarize our recent progress with functional biosupramolecular systems concisely. The functions covered are artificial photosynthesis, anion transport, and sensing in lipid bilayer membranes. With artificial photosynthesis, the current emphasis is on the construction of ordered and oriented architectures on solid surfaces. Recent examples include the zipper assembly of photosystems with supramolecular n/p-heterojunctions and oriented antiparallel redox gradients. Current transport systems in lipid bilayers reveal new interactions at work. Examples include anion−macrodipole or anion−π interactions. Current attention with membrane-based sensing systems shifts from biosensor approaches with enzymatic signal generation to aptamers (i.e., the DNA version of immunosensing) and differential sensing with dynamic polyion−counterion transporters. The functional diversity accessible with biosupramolecular systems is highlighted, as is the critical importance of cross-fertilization at intertopical convergence zones.

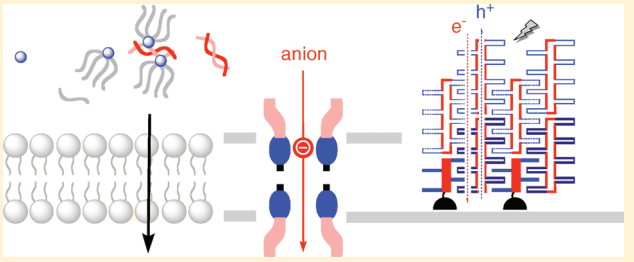

INTRODUCTION

This account summarizes recent key contributions from this group to biosupramolecular systems with interesting functions.[1−7] In functional supramolecular systems, more than one molecule works together to achieve activity. The individual molecules alone are inactive or at least less active. In biosupramolecular systems, lessons from nature are used one way or another to create or improve activity. The unifying theme of this account is transport. We start as small as possible with the transport of electrons in supramolecular photosystems on solid surfaces.[1−3] Then we move on from electrons to the transport of anions across lipid bilayer membranes, focusing on the use of anion−π interactions.[4,5] Finally, we finish as large as possible and describe how the ability of supramacromolecular polyion−counterion complexes to move across lipid bilayers can be used to build aptamerosensors[6] and differential sensing systems.[7]

An important objective with artificial photosynthesis is to apply lessons from nature to the design of organic solar cells.[8−12] Recent artificial photosystems that work like biological photosystems in bilayer membranes include transmembrane helical π stacks that can open up into ion channels in response to the intercalation of ligands.[13] In another example, active electron transport with light is coupled with selective anion antiport.[14] The resulting electroneutral photosystems are of interest in avoiding membrane polarization and saturation at low turnover.

To apply lessons from biological and artificial photosystems in lipid bilayers to organic solar cells, new methods of constructing ordered and oriented biosupramolecular architectures on solid surfaces are needed.[8−11] Today, commercial solar cells mostly use inorganic materials, particularly silicon. However, organic solar cells[12] and dye-sensitized solar cells[15] are attracting more and more attention as potentially interesting alternatives. Current organic solar cells have either bilayer or bulk n/p-heterojunction (BHJ) architecture.[8−12] In bilayer solar cells, macroscopic layers of electron (e^-, n)-transporting and hole (h^+, p)-transporting materials are deposited next to each other. In BHJs, these two layers are mixed up to increase their interfacial area. The resulting improvements in photoinduced charge separation usually come at the cost of reduced charge mobility in the more disordered layers. Supramolecular n/p-heterojunctions (SHJs) have been proposed to unify the advantages of bilayer and BHJ architectures without suffering from the corresponding shortcomings.[8−11] Like biological photosystems, SHJs are envisioned to contain hole- and electron-transporting pathways on the molecular level. These n- and p-type channels are aligned coaxially to maximize the n/p-interface. This arrangement should maximize photoinduced charge separation without losses in charge mobility. Today, operational SHJs still remain to be discovered despite much effort worldwide. This slow progress originates in part from the formidable synthetic organic and supramolecular chemistry challenges involved.[8−11] Nevertheless, lessons from nature suggest further equipping SHJs with antiparallel redox gradients to drive the charges apart right after their generation and collect solar energy without any losses from charge recombination.[8] Preliminary results in this direction will be summarized in the following text.[3]

In clear contrast to the open questions concerning the transport of electrons in SHJ photosystems, the transport of

Received: February 15, 2011
Revised: March 21, 2011
Published: April 13, 2011

dx.doi.org/10.1021/la200593p | *Langmuir* 2011, 27, 9696–9705

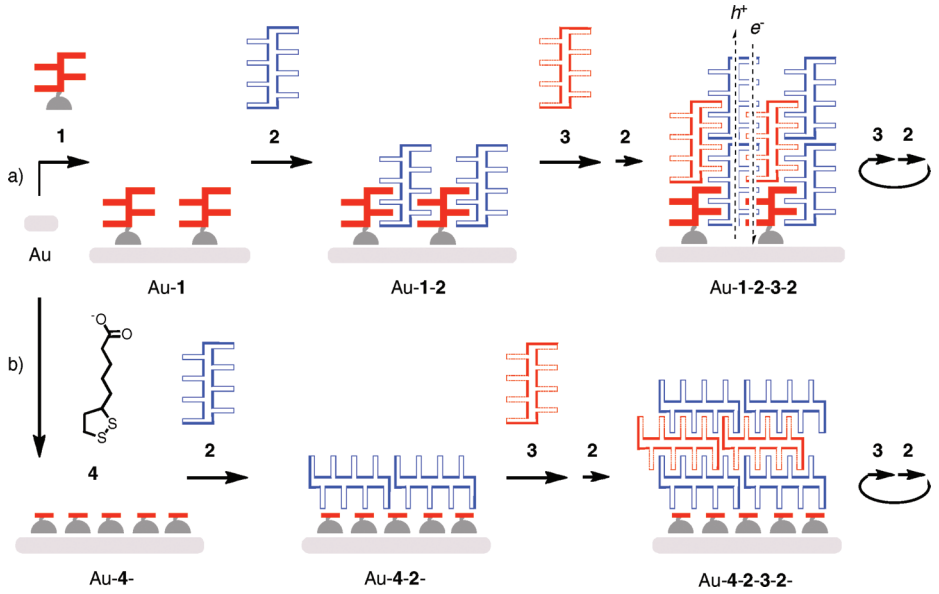

Figure 1. (a) Zipper assembly and (b) layer-by-layer (LBL) assembly on gold. See Figure 2 for structures.

ions across lipid bilayer membranes can be considered to be almost routine today.[16−19] Over the years, this group has contributed a broad variety of structural motifs including artificial β-barrels,[20] helical π-stacks,[13,21] rigid-rod π-slides,[14] push−pull rods,[22−25] dendritic folate quartets,[26] and stacked nanotubes.[27] These motifs provided access to functional characteristics such as voltage gating,[22,24] ligand gating,[13,21] blockage,[20,28−33] catalysis,[34] pH gating,[35] ion selectivity,[35,36] and so on. Recent efforts in the group focus on the expansion of the repertoire of interactions available to create function. Early examples of this topic include hydrogen-bonded chains and cation−π interactions for proton and potassium transport, respectively.[36,37] More recent contributions include aromatic electron donor−acceptor interactions,[13,21,32,33] anion−macrodipole interactions,[27] "dynamic" polyion−counterion pairing,[6,7] and anion−π interactions.[4,5,37] The resulting inversion of the paradigm of using ion-transport systems as a tool to catch otherwise elusive interactions at work will be described in the following text.[4,5]

The idea to use synthetic transport systems as sensors is an obvious one considering that our own tongues and noses operate with responsive pores in lipid bilayer membranes. Stochastic or immunosensing with native or bioengineered pores was realized early on.[38] However, the construction of purely synthetic sensing systems that work in complex matrices from the supermarket or hospital has been difficult. The first step in this direction concerned the synthesis of stimuli-responsive transporters that can function as signal transducers.[28] The next step was their combination with enzymes to generate analyte-specific signals.[29−31] In a third step, signal amplifiers were introduced as bifunctional molecules that can capture the product of enzymatic signal generation on one hand and ensure the responsiveness of the synthetic transport system on the other hand.[32,33] Recent efforts to complement this biosensing approach with aptamerosensing[6] and differential sensing[7] approaches will be described in the following text.

More detailed reviews on specific aspects of functional biosupramolecular systems are available.[8,20,37] Here, we will move on with a more general overview to elaborate on the latest development in the group. We will focus on artificial leaves first, followed by ion transport with anion−π interactions and artificial noses and will conclude with a few comments on the importance of functional feedback loops, intertopical convergence zones, and cross-fertilization.

■ ARTIFICIAL PHOTOSYSTEMS

The construction of ordered and oriented biosupramolecular systems on solid surfaces is a central challenge in materials science. Methods involving solution processing usually fail to achieve directionality, lateral self-sorting, molecular-level precision, and so on.[8−13] Available methods that directly build on surfaces, notably surface-initiated polymerization[39,40] and layer-by-layer (LBL) assembly,[41,42] usually suffer from poor organization, including lateral self-sorting and an incompatibility with much relevant chemistry.

To contribute to our learning on how to build on solid ground in an ordered and oriented manner, we have introduced a zipper assembly (Figure 1a).[43,44] The construction of Au-**1**-(**2**-**3**-)$_n$ as a representative example begins with the deposition of initiator **1** on gold (Figure 1a).[1−3] Initiator **1** contains a short *p*-oligophenyl (POP) scaffold that is decorated with negatively charged naphthalenediimides (NDIs)[44,45] without substituents in the core (Figure 2). A strained disulfide is added at one terminus to bind to gold. To the obtained Au-**1** monolayers, propagator **2** is added. Propagator **2** is equipped with a scaffold of double length and positively charged, yellow, core-substituted NDIs (cNDIs).[45−48] Multiion pairing and flanking hydrogen-bonded chains direct the lower half of the cationic cNDIs to interdigitate within the anionic NDIs of the initiator and form π-stacks. The upper half of the cNDIs remains free on the surface of bilayer Au-**1**-**2**, like sticky ends in DNA biotechnology (see below). These sticky ends then zip up with the lower half of the anionic cNDIs of propagator **3**. Repeated zipping of the two complementary propagators then affords final zipper architecture Au-**1**-(**2**-**3**-)$_n$. The less organized, classical LBL assemblies[41,42] Au-**4**-(**2**-**3**-)$_n$ are prepared from anionic monolayers of Au-**4**. LBL architecture

dx.doi.org/10.1021/la200593p |*Langmuir* 2011, 27, 9696–9705

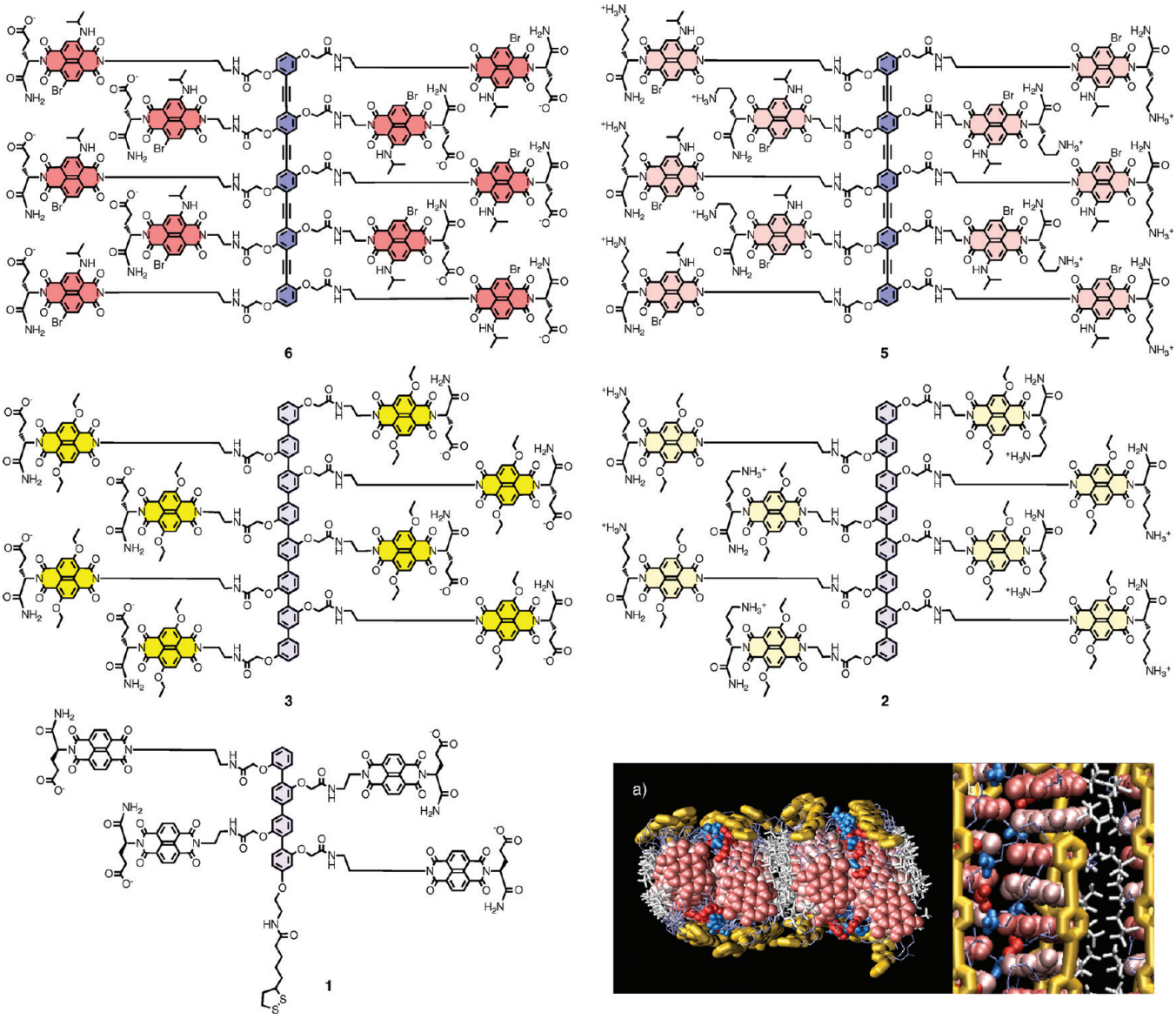

Figure 2. Structure of all components used for the zipper assembly of artificial photosystems, including OMARG SHJs (Figures 1 and 3−5). NDIs in **5** and **6** are mixtures of 2,6- and 3,7-regioisomers. (a, b) MD simulations of zipper architecture -(**5**-**6**-)$_n$- in (a) axial and (b) side views. cNDI stacks are shown in garnet; rods, in gold; isopropyl domains, in silver; and ion pairs, in red and blue. Reproduced with permission from ref 3. Copyright 2010 American Chemical Society.

Au-**4**-(**2**-**3**-)$_n$ is of interest as a negative control to work out the special characteristics of zipper architecture Au-**1**-(**2**-**3**-)$_n$.

One objective of the zipper assembly was to create SHJ photosystems with n-type π-stacks that grow along strings of p-type rods perpendicular to the surface (Figures 1a and 2a). For this purpose, stacks and scaffolds have been varied extensively, including the red cNDIs and the oligophenylethynyl (OPE) scaffolds in cationic and anionic propagators **5** and **6** (Figure 2).[2] Molecular models of -(**5**-**6**-)$_n$- confirmed the coaxial alignment of n-stacks along strings of p-rods (Figure 2b).[3] The top view further highlights how the π-stacks are put in place by alternating hydrophobic domains (silver) as well as multiple interstack ion pairing (blue and red, Figure 2a).

Compared to LBL photosystems, zipper architectures generally produce much more photocurrent (Figure 3), have smoother surfaces, and are responsive to functional controls (e.g., capping).[1,2] Slow assembly kinetics (1−3 days against hours for LBL) indicates the occurrence of extensive error correction and self-repair during zipper assembly.[1] The critical thickness of zippers, that is, the thickness where the photocurrent stops increasing, was generally better than the critical thickness of LBL assemblies.[1,2] Quartz crystal microbalance (QCM) controls showed linear growth that was well beyond the critical thickness for both approaches. Better critical thickness thus demonstrates that zipper architectures achieve photoinduced charge separation over longer distances, (SPR data confirmed that 50 layers, as in Figure 4c, corresponds to ∼90 nm). This reduced charge recombination confirms the functional relevance of the supramolecular organization obtained by the zipper assembly.

The functional relevance of zipper architectures was further confirmed by consistently high fill factors in current−voltage ($J-V$) profiles (Figure 3).[1,50] All photocurrent measurements

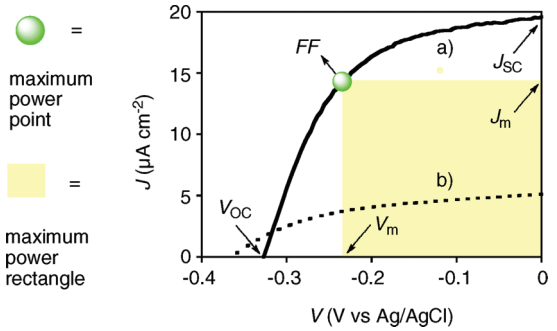

Figure 3. Current−voltage profile of (a) zipper Au-**1**-(**2**-**3**-)$_9$-**2** (solid) and (b) LBL Au-**4**-(**2**-**3**-)$_9$-**2** recorded with the photosystems as the anode, a Pt electrode as the cathode, and triethanolamine (TEOA) as a mobile electron donor in 100 mM aqueous Na_2SO_4. The short circuit current density (J_{SC}), open circuit voltage (V_{OC}), maximum power rectangle (yellow), maximum power point (green), and fill factor FF = maximum power/($V_{OC} \times J_{SC}$) = ($V_m \times J_m$)/($V_{OC} \times J_{SC}$) are indicated. Reproduced with permission from ref 1. Copyright 2009 American Chemical Society.

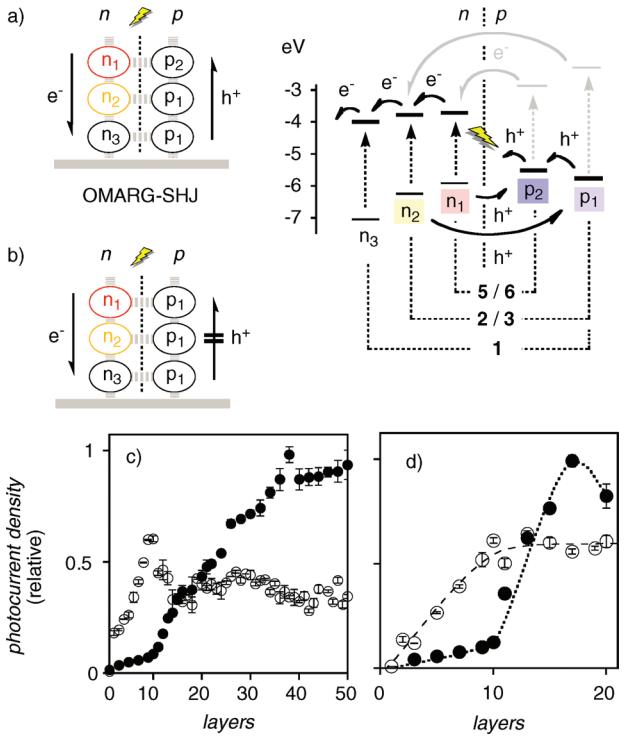

Figure 4. (a) Formal OMARG-SHJ architecture Au-**1**-(**2**-**3**-)$_m$-(**5**-**6**-)$_n$- with HOMO/LUMO levels for photoinduced (dashed arrows) e^- (gray) and h^+ injection (black) into n- and p-type transporting pathways (bold). (b) Control without a gradient in the p-channel. (c) Current-layer profile of Au-**1**-(**2**-**3**-)$_4$-**2**-(**6**-**5**-)$_n$- (●) and anti-OMARG-SHJ Au-**1**′-(**5**-**6**-)$_4$-**5**-(**3**-**2**-)$_n$- (○). (d) The same for single-channel control (●) and the corresponding antisystem (○). Reproduced with permission from ref 3. Copyright 2010 American Chemical Society.

were made in a wet system with mobile carriers as in dye-sensitized solar cells.[15] The fill factor FF = $J_{mp} \times V_{mp}/J_{SC} \times V_{OC}$ describes the nonlinearity of the $J-V$ curve and is an important contributor to the maximal output power P_{max} (= FF × J_{SC} × V_{OC}). Linear (ohmic) $J-V$ curves have FF_{min} = 0.25, and optimized BHJ solar cells have FF ≈ 0.61.[12,50] FF = 0.50−0.60 obtained with zippers is important considering that FF increases with increasing thickness.

In biological photosystems, electrons and holes, after being separated with light, move along molecular-level channels in a directional manner so as never to meet each other again and recombine.[8] This directionality is obtained by spacially orthogonal multicomponent redox gradients. The application of these lessons from nature suggests that what we really would like to build and explore are OMARG-SHJs (i.e., multicolored SHJs with oriented antiparallel redox gradients). OMARG-SHJs should harvest as much light as possible, separate charges at maximized n/p-interfaces, and direct them in opposite directions to collect photonic energy without losses from charge recombination.[8] The first formal OMARG-SHJ photosystem was prepared last year using the zipper assembly (Figure 4).[3] To get there, the yellow cNDI domains built along POP scaffolds in Au-**1**-(**2**-**3**-)$_n$ were covered with red cNDI domains around the OPE scaffolds of **5** and **6**. This Au-**1**-(**2**-**3**-)$_n$-(**5**-**6**-)$_m$- architecture creates redox gradients in the cNDI stacks that direct electrons toward the gold surface (Figure 4a). Driven by the POP → OPE gradients, the holes cannot follow and move into the opposite direction instead. Moreover, holes can be injected everywhere from excited cNDIs into the p-channels. The same is in principle possible for electron injection from excited OPEs or POPs into the n-type transporting pathways. Assuming the functional irrelevance of the few NDI n_3's in initiator **1**, this design affords a minimalist OMARG-SHJ with antiparallel gradients composed of two components each.

The current-layer profile of OMARG-SHJ Au-**1**-(**2**-**3**-)$_4$-**2**-(**6**-**5**-)$_n$- is shown in Figure 4c (●).[3] The sharp increase in photocurrent upon the transition from yellow to red domains in the 11th layer originates from the intrinsic ability of red photosystems -(**5**-**6**-)$_n$- to generate more photocurrent than yellow photosystems -(**2**-**3**-)$_n$- and has nothing to do with redox gradients. Photocurrent generation continued to increase with continuing growth of the red domain beyond 40 layers. This is a critical thickness that is more than twice the up to 20 layers obtained with gradient-free zippers. According to QCM, photocurrent saturation with OMARG-SHJ Au-**1**-(**2**-**3**-)$_4$-**2**-(**6**-**5**-)$_n$- above 40 layers occurs not because the zipper assembly stops growing. Moreover, photocurrent saturation does not occur because of the onset of charge recombination. It simply occurs because all of the photons are used at this thickness. We conclude that already minimalist OMARG-SHJ photosystems with two-component gradients suffice to separate charges over formally infinite distances.

Anti-OMARG-SHJ Au-**1**′-(**5**-**6**-)$_4$-**5**-(**3**-**2**-)$_n$- with misaligned antiparallel gradients initially generates a large amount of photocurrent because of the good performance of the red domain (Figure 4c, ○).[3] The yellow domain partially inhibits photocurrent generation down to a constant residual level. This residual photocurrent implies the occurrence of two-photon pumping against the redox gradients. Redox gradients with more than two components should be able to cause full photocurrent inhibition in anti-OMARG-SHJs.

The removal of one gradient in the original OMARG-SHJ reduces the critical thickness down to 15 layers (Figure 4b,d, ●).[3] This finding confirmed that both gradients are needed for photoinduced charge separation over "infinite" distances with OMARG-SHJs. With one gradient only, electrons are driven in one direction but holes can follow, diffuse in the same direction,

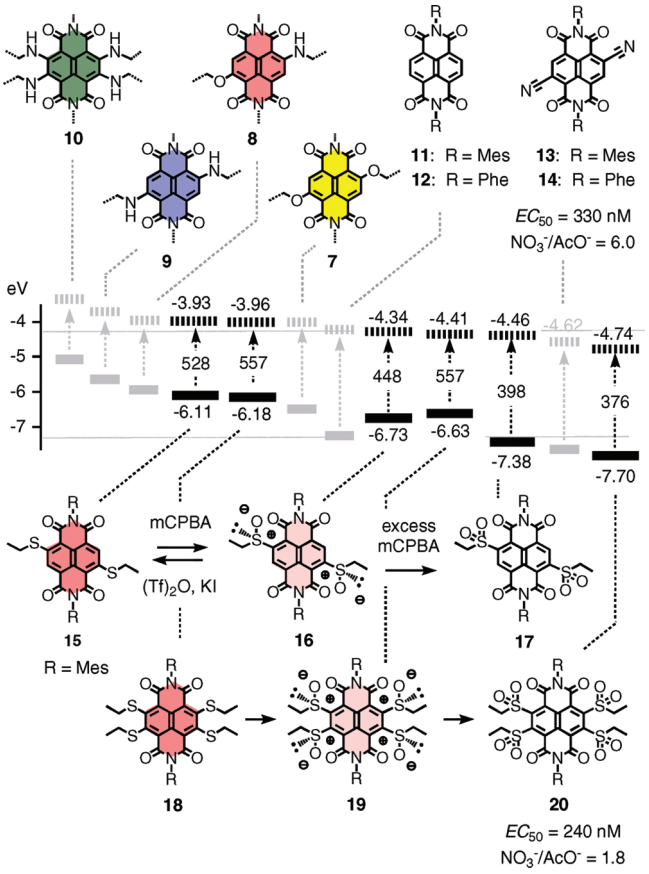

Figure 5. Frontier orbital energies, absorption maxima, anion-transport activity, and selectivity of selected cNDIs. HOMO (bold) and LUMO (dashed) energies are in electronvolts against vacuum (−5.1 eV for Fc/Fc$^+$), absorption maxima are in nanometers (dashed arrows), and transport activities are in EC_{50} (effective concentration for 50% activity; Mes, mesityl; Phe, phenyl; see Figure 6).

and recombine anywhere. Photocurrent inhibition in the corresponding antisystems with single gradients fails for the same reason (Figure 4d, ○).

The obtained activities suggest that zipper assembly provides access to ordered and oriented architectures that are otherwise far beyond reach, including the first OMARG-SHJ photosystem. However, the zipper assembly will never be useful in practice because the organic synthesis involved is much too demanding. Current efforts focus on fast, cheap alternatives to zipper assembly that can provide access to similarly important activities without extensive synthesis efforts.[51]

■ ANION−Π INTERACTIONS AT WORK

Efforts to expand the repertoire of noncovalent interactions available to construct new biosupramolecular systems with significant functions are of fundamental importance.[4,5] To generate function, weak interactions are usually sufficient and often preferable. Strong interactions tend to freeze rather than enable processes such as molecular translocation or transformation. However, a demonstration of the functional relevance of weak interactions can be difficult because routine methods report strong interactions only. In a paradigm inversion, we have considered assays for ion transport across lipid bilayer membranes as a new tool for catching unusual interactions at work.

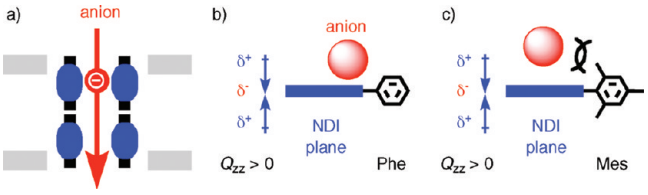

Figure 6. (a) Hypothetical NDI bundles for anion-transport across lipid bilayers with anion−π interactions. Peripheral substituents modulate (b) more- and (c) less-favorable anion−π interactions as well as the self-assembly into active NDI bundles (not shown).

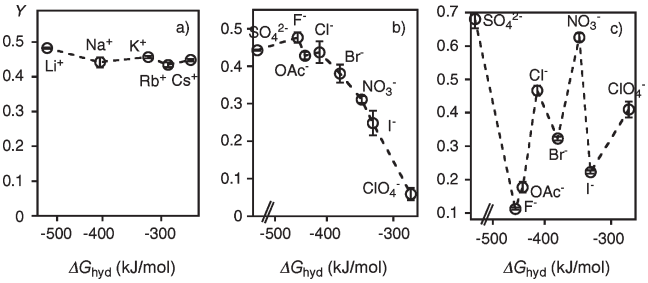

Figure 7. Dependence of the transport activity Y of NDIs (a, b) **12** and (c) **14** on the hydration energy of (a) cations and (b, c) anions in the buffer. Reproduced with permission from ref 4. Copyright 2010 Nature Publishing Group.

This approach has been applied to hydrogen-bonded chains,[36] polyion−counterion pairing,[6,7] aromatic electron donor−acceptor (charge-transfer) interactions,[13,21,32,33] anion−macrodipole interactions,[27] and dynamic covalent capture.[7,32,33,52,53] The most recent highlight in this series concerns anion−π interactions with core-substituted naphthalenediimides (cNDIs).[4,5,46]

As mentioned in the previous section, π-donors in the core transform cNDIs into colorful building blocks for artificial photosystems.[46−49] cNDI **7** with two alkoxy donors in the core is a yellow-blue emitting fluorophore (Figure 5). The replacement of single oxygen by a nitrogen produces red-orange fluorescent cNDI **8**. The substitution of the second oxygen by another nitrogen gives blue-red fluorescent cNDI **9**, and four alkylamino donors give green cNDI **10**. Such accessibility to all primary colors by single-atom substitution, without global structural changes, is ideal for the construction of multicomponent architectures. Rising HOMO/LUMO levels with a decreasing band gap is perfect for building OMARG-SHJs without low-energy traps.[3,8]

With π-acceptors in the core, cNDIs become strong π-acids.[46] This is interesting because only π-acids with an inverted quadrupole moment, $Q_{ZZ} > 0$, can enjoy anion−π interactions (Figure 6).[54−56] Unsubstituted NDIs (e.g., **11** and **12**) are among the strongest π-acids known today. Their $Q_{ZZ} = +19$ B is similar to TNT and more than twice that of hexafluorobenzene, and their LUMO energy is at −4.31 eV (Figure 5). Two cyano π-acceptors in the core of cNDIs as in **13** or **14** double the quadrupole moment to an unprecedented $Q_{ZZ} = +39$ B and lower the LUMO to −4.62 eV (Figure 6).

We have previously considered anion−π interactions for the construction of transport systems in lipid bilayer membranes.[14,37] However, we consistently failed to prove that anion−π interactions really account for function. Possible contributions from hydrogen bonding and ion pairing could never be

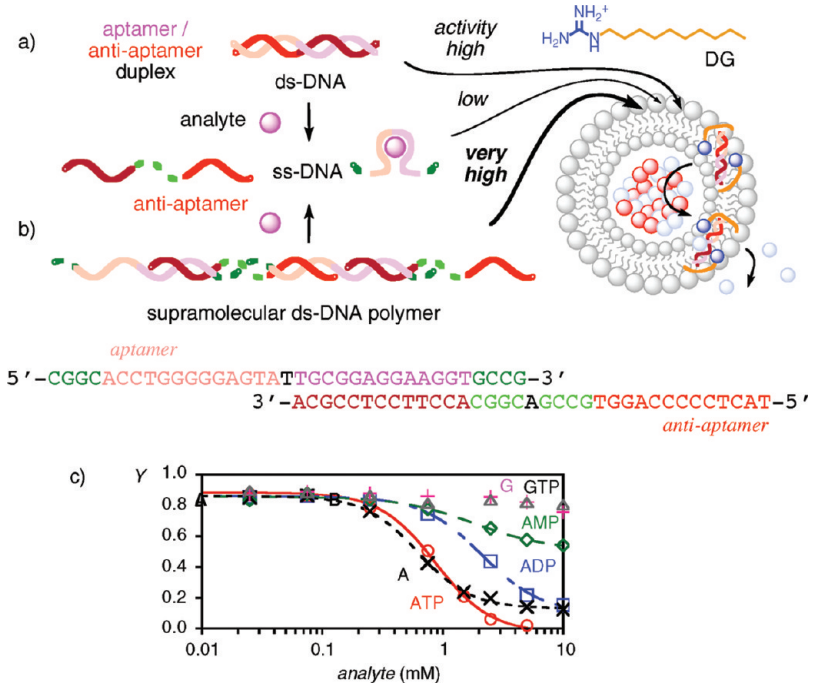

Figure 8. Sensing with aptamers in fluorogenic vesicles. Disassembly of aptamer/antiaptamer duplexes (a) without or (b) with sticky ends in response to analyte binding converts ds-DNA and supramolecular ds-DNA polymers with high to very high activity into poorly active ss-DNA. (c) Dose response curves for nucleotide discrimination by the original ATP aptamer adapted to operate as a transporter in lipid bilayers. Adapted with permission from ref 6. Copyright 2009 American Chemical Society.

excluded for sure. To uncover the truth, a series of minimalist NDIs were prepared where nothing was left for anions to interact with except a π-acidic surface.[4] Direct evidence for anion binding by NDIs **11** and **12** and cNDIs **13** and **14** was obtained by laser-induced tandem mass spectrometry fragmentation studies with heterodimeric chloride complexes. The anion affinity increased with increasing π-acidity (**13**, **14** > **11**, and **12**) and active site decrowding (**12**, **14** > **11**, and **13**). Identical trends in theoretical calculations and ion-transport activity confirmed the functional relevance of anion$-\pi$ interactions.

In ion-transport experiments, insensitivity toward cation exchange and sensitivity toward anion exchange confirmed that NDIs transport anions (Figure 7).[4] The decreasing activity of NDI **12** with respect to transporting anions with a decreasing dehydration penalty, so-called anti-Hofmeister behavior, can be interpreted as strong anion binding by the active supramolecular system with little selectivity (Figure 7b). Increasing π-acidity of the most active cNDI **14** enhanced nitrate and suppressed acetate transport on this anti-Hofmeister background (Figure 7c). Increasing nitrate over acetate selectivity with increasing π-acidity and supramolecular organization suggested that anion$-\pi$ interactions are enhanced by $\pi-\pi$ interactions with planar oxyanions.

Efforts to synthesize tetracyano NDIs with a spectacular Q_{ZZ} = +55 B failed despite significant effort.[4] Nevertheless, to synthesize "super-π-acids" in the NDI series, cNDI **15** with two sulfides in the core was reversibly oxidized first to sulfoxide **16** and then to sulfone **17** (Figure 5).[5] To increase the π-acidity further, cNDI **18** with four sulfides in the core was synthesized and oxidized to tetrasulfoxide **19** and tetrasulfone **20**. Cyclic voltammograms revealed that the two sulfones in the core of **17** generate 160 meV less π-acidity than two cyano groups of **13**. However, with a LUMO at −4.74 eV, tetrasulfone **20** is by 120 meV the most π-acidic cNDI known today. The anion-transport activity of super-π-acid **20** is naturally outstanding (EC_{50} = 240 nM) despite the interference from peripheral methyl groups (Figure 5).

There is no reason that lessons learned on the recognition and translocation of anions in the ground state should not be applicable to transition-state stabilization.[4,5] cNDIs with chiral sulfoxides in the core are particularly attractive with regard to asymmetric catalysis by means of anion$-\pi$ interactions.[5] Ongoing efforts toward anion$-\pi$ catalysis are complemented by studies on transport with halogen bonds, a similarly underexplored interaction in biosupramolecular systems chemistry (beyond tyroid glands).[57]

SENSING IN LIPID BILAYERS

Multiion hopping on and by polyions such as DNA, RNA, and cell-penetrating peptides has been used previously for cellular uptake and biosensing.[58,59] However, enzymatic signal generation in biosensing approaches is limited by the availability of specific enzymes.[29−33,59] To overcome this limitation, aptameric immunosensing[6] and differential sensing methods[7] have been explored recently for the first time in the context of sensing systems that operate in lipid bilayer membranes. Both methods are universal and adaptable to any analyte of choice.

In immunosensing, signal generation is general because antibodies can be prepared against virtually any analyte.[38] Aptamers are the DNA version of antibodies with advantages including in vitro preparation by DNA biotechnology (rather than in mice).[6] In membrane-based sensing systems, DNA aptamers could serve as both the signal generator and signal transducer. Signal transduction with DNA aptamers was conceivable because

dx.doi.org/10.1021/la200593p |*Langmuir* 2011, 27, 9696–9705

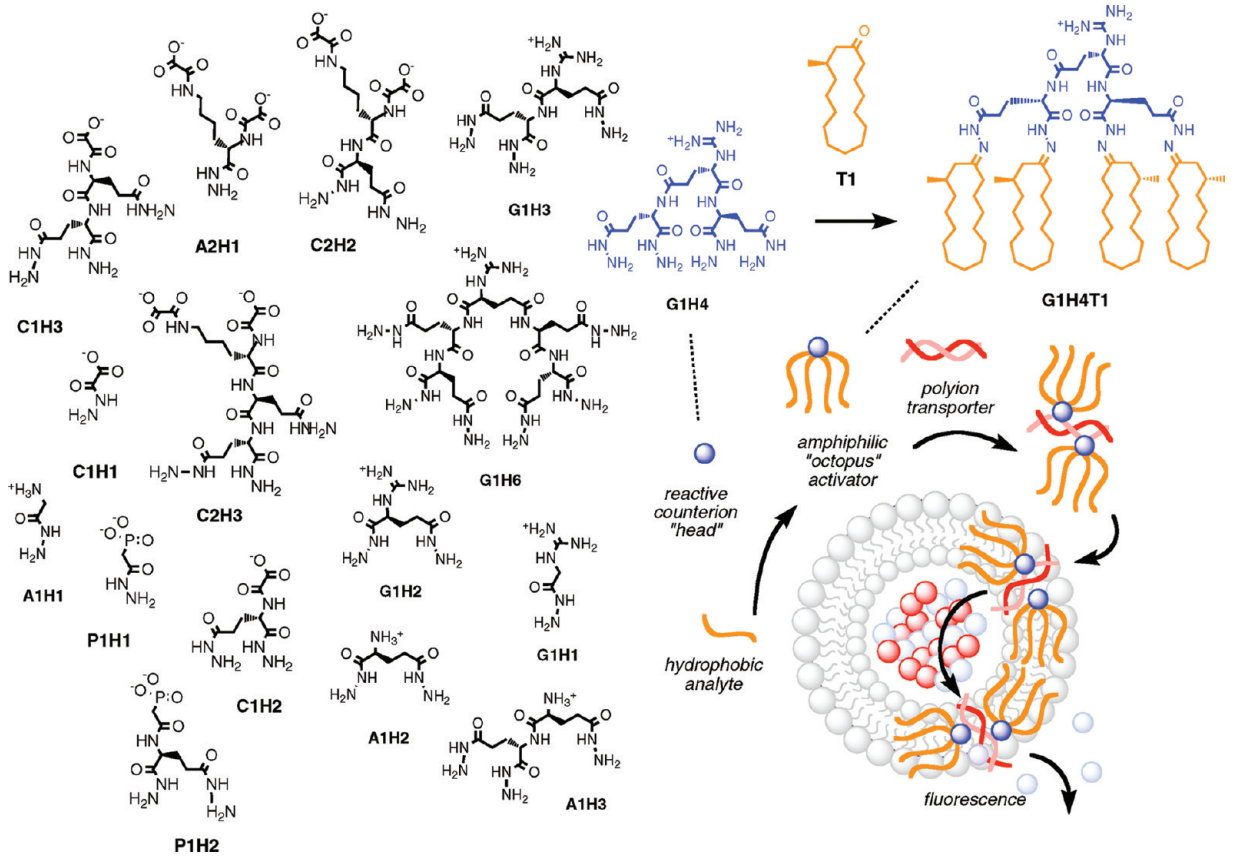

Figure 9. Sensing scheme for the differential sensing of hydrophobic analytes with counterion-activated polyion transporters in fluorogenic vesicles. For sensing with polyanionic DNA, hydrophobic analytes (e.g., muscone **T1**) are incubated with reactive hydrophilic cations (e.g., **G1H4**), the resulting amphiphile **G1H4T1** acts as a counterion activator of DNA transporters, and their activity is recorded as fluorescence recovery during the release of cationic fluorophores or quenchers from the vesicle. For sensing with polycationic cell-penetrating peptides (CPPs), analytes are incubated with reactive hydrophilic anions such as **C2H2**.

amphiphilic counterions such as dodecylguanidinium (DG) have been shown recently to activate DNA as cation transporters in bulk and lipid bilayer membranes (Figure 8).[58] However, the transport activity of short ss-DNA aptamers including the original ATP aptamer turned out to be very low and insensitive to the presence of the analyte ATP.[6]

Aptamer/antiaptamer duplexes gave increased activity and responsiveness because duplex disassembly upon analyte binding inactivates the transporter.[6] However, the big breakthrough came with the application of sticky-end technology to polymerize the aptamer/antiaptamer duplexes. In the presence of the analyte, the highly active supramolecular ds-DNA polymers disassemble into inactive ss-DNA. The final, high-contrast sensing system perfectly reproduces the (poor) sensitivity and the (interesting) selectivity of the original ATP aptamer, operating here as a cation transporter in lipid bilayer membranes.

Aptamerosensors, immunosensors, biosensors, and related sensing systems will never be capable of discriminating more than 10 000 analytes with ~350 signal generators. This is the sensing power of mammalian olfactory systems.[7] Rather than aiming for 1:1 recognition of every individual analyte, multiple membrane-based receptors with less specificity are used to generate patterns that are then analyzed in the brain. This so-called differential sensing strategy has been applied to about every existing chemosensor systems except, ironically, the ones that operate like olfactory receptors in lipid bilayer membranes.[7,60−62]

The problem with membrane-based sensing systems has been the production of a sufficient number of cross-responsive sensing elements. To change this situation and rapidly produce small collections of sensing systems, dynamic polyion−counterion transporters have been introduced.[7]

This approach is ideal (but not exclusive) for hydrophobic analytes as "tails" (e.g., "Geneva" odorant muscone **T1**, Figure 9).[7] Covalent capture by cationic (or anionic) hydrazide "heads" (e.g., **G1H4**) produces cationic amphiphiles (e.g., **G1H4T1**) that in turn can act as countercation activators for polyanionic transporters in fluorogenic vesicles.[7,63−65] To expand the dimension of signals generated by this system, we prepared a collection of small peptides containing one to three positive (**G**, guanidinium; **A**, ammonium) or negative charges (**C**, carboxylate; **P**, phosphonate) and one to four reactive hydrazides (**H**). Odorants such as **T1**−**T13** are wonderful examples of hydrophobic analytes. Calf-thymus DNA has been used as representative polyanion and cell-penetrating peptides (CPPs),[65−68] such as polyarginine as a representative polycation. In general, guanidinium cations were better activators than ammonium cations, and carboxylates were better than phosphonates. With DNA, the activity increased with an increasing number of tails until octopus amphiphile **G1H4T** was obtained, whereas CPPs performed best with gemini amphiphiles obtained from **C2H2**.

The different activities obtained with different headgroups generated multidimensional patterns for each analyte.[7] Standard

dx.doi.org/10.1021/la200593p |*Langmuir* 2011, 27, 9696–9705

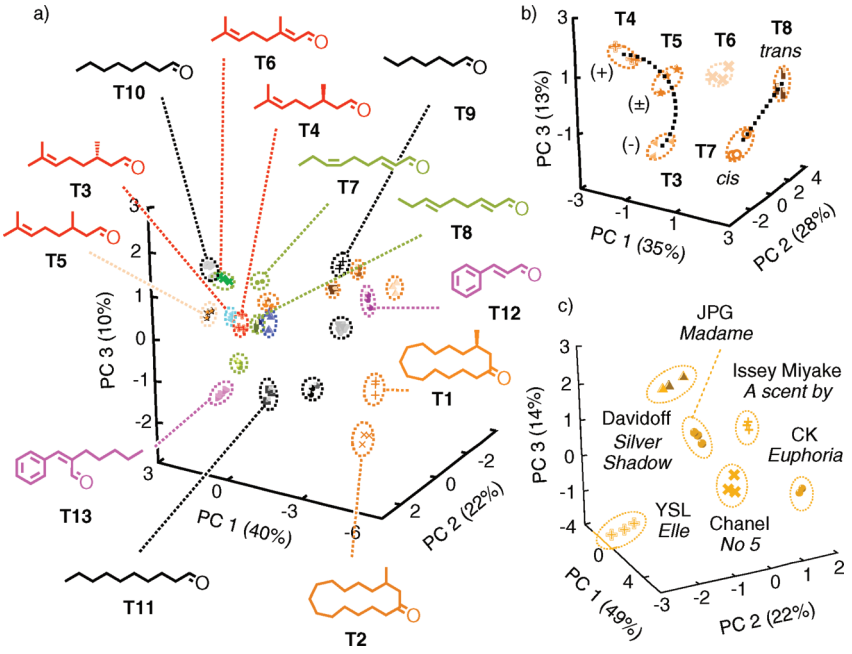

Figure 10. Differential sensing with dynamic polyion−counterion transport systems. Principal component analysis (PCA) score plots for odorants and perfumes. PC 1−PC 3 describes the first three principal components, covering the corresponding percentage of data variance. Data points represent independent experiments with DNA sensors and counteranions **G1H3**, **G1H2**, **A1H3**, and **A1H3** (Figure 9). (a) Global PCA score plot for 21 odorants. (b) Focused PCA score plot highlighting enantiodiscrimination and cis−trans isomerization. (c) PCA score plot for selected perfumes. Adapted from ref 7 by permission of The Royal Society of Chemistry.

methods including principal component (PCA) and hierarchical cluster analysis were applied to pattern recognition. PCA concentrates the most relevant characteristics of multidimensional patterns into a virtual 3D space (Figure 10). This is achieved by calculating eigenvectors (principal components, PC) in the direction of maximal variances to obtain a single score that can be plotted in the new PC space. At least 21 analytes were readily discriminated in global PCA score plots (Figure 10a). Sorted in descending order, 40% of the data variance in PC 1 and 22% in PC 2 added up to 64% of the data variance, whereas 81% of the data variance was accounted for in virtual 3D space. These comparably low values are interesting because they demonstrate that several different interactions contribute to the sensing power of the system. Structurally very similar analytes were discriminated without problem, including enantioenriched and racemic muscone **T1** and **T2**, respectively, citronellal enantiomers **T3** and **T4**, their racemate **T5**, and the closely related citral **T6** or the green cucumber aldehyde **T7** and the all-*trans* **T8** isomer. Single-carbon homologues such as **T9**−**T11** were not problematic, not to mention less similar odorants including cinnamaldehyde **T12** and jasminaldehyde **T13**.

Apparent clusters in global PCA score plots could be readily resolved by PCA focusing (Figure 10b). Inverse detection protocols were developed to sense analytes as small as acetone. Perfumes were selected as appealing example of complex mixtures to demonstrate the compatibility of our biosupramolecular nose with real-life samples.

CONCLUSIONS

The objective of this account was to wrap up recent progress with functional biosupramolecular systems. Functions of current interest include artificial photosystems, ion transporters, and sensors that work in lipid bilayer membranes. Recent highlights include photoinduced charge separation over infinite distances by the first multicolored photosystems with oriented supramolecular n/p-heterojunctions and antiparallel redox gradients (so-called OMARG-SHJs).[3] Other milestones concern unprecedented evidence of the functional relevance of anion−π interactions[4] or the first synthetic sensing system that works, like mammalian olfactory systems, by pattern generation in lipid bilayer membranes.[7]

This account also illustrates the importance of cross-fertilization at intertopical convergence zones to identify significant questions and aim for innovation on the conceptual level, not to speak of educational value and scientific breath. Examples include sticky-end technology, essential not only for sensing with aptamers in lipid bilayers[6] but also for building oriented and ordered photosystems on solid grounds (e.g., OMARG-SHJs)[1−3] or polymerizing coiled-coil dimers into protein fibers.[69] Dynamic multiion pairing is confirmed as a powerful tool for building functional systems on surfaces and in lipid bilayer membranes as shown in zipper architectures[1−3] and polyion−counterion transporters,[6,7] respectively. Dynamic covalent chemistry[52,53] has been the key to generating the small collections of functional systems that are needed to achieve differential sensing in lipid bilayers.[7] The same dynamic covalent chemistry will be essential to create ordered and oriented multicomponent photosystems that are as sophisticated as zipper assemblies but much easier to synthesize.[51] From a structural point of view, panchromatic cNDI[46−49] fluorophores with π-donors in the core are perfect for artificial photosynthesis,[1−3] whereas the super-π-acids obtained with π-acceptors are ideal for transporting electrons as well as anions.[4,5]

Broader perspectives in the field have been described elsewhere and should not be repeated where they do not belong.[70]

dx.doi.org/10.1021/la200593p |*Langmuir* 2011, 27, 9696–9705

This account supports the idea that multidisciplinary thinking will be important in identifying very important questions in intertopical convergence zones and in finding very important answers by intertopical cross-fertilization. For instance, we have to learn how to build multicomponent architectures at physical and biological interfaces not only with molecular-level precision but also with user-friendly building blocks. This is a general challenge where supramolecular chemistry can make a difference in building the materials of the future and addressing large global problems. The need to achieve increasingly important activities with increasingly accessible building blocks calls for a shift in attention toward multicomponent systems. The development of new strategic concepts such as self-sorting for their construction will be crucial. Complex systems have been underexplored in the past because they cannot be characterized on the structural level.[70] Applying another fundamental lesson from biology and biotechnology, functional feedback loops will have to replace structural feedback as the first priority.[70] This account supports functional feedback loops as a fruitful and reliable strategy that becomes increasingly powerful with the increasing complexity of the systems involved.

AUTHOR INFORMATION

Corresponding Author

*Home page: www.unige.ch/sciences/chiorg/matile/. E-mail: stefan.matile@unige.ch.

ACKNOWLEDGMENT

We warmly thank all past co-workers and past and present collaborators for their contributions and the University of Geneva, NCCR Chemical Biology, and the Swiss NSF for financial support. J.A. acknowledges a Marie Curie Fellowship, E.O. is a Sciex Fellow, and S.M. is an ERC Advanced Investigator.

REFERENCES

(1) Kishore, R. S. K.; Kel, O.; Banerji, N.; Emery, D.; Bollot, G.; Mareda, J.; Gomez-Casado, A.; Jonkheijm, P.; Huskens, J.; Maroni, P.; Borkovec, M.; Vauthey, E.; Sakai, N.; Matile, S. *J. Am. Chem. Soc.* **2009**, *131*, 11106–11116.

(2) Bhosale, R.; Perez-Velasco, A.; Ravikumar, V.; Kishore, R. S. K.; Kel, O.; Gomez-Casado, A.; Jonkheijm, P.; Huskens, J.; Maroni, P.; Borkovec, M.; Sawada, T.; Vauthey, E.; Sakai, N.; Matile, S. *Angew. Chem., Int. Ed.* **2009**, *48*, 6461–6464.

(3) Sakai, N.; Bhosale, R.; Emery, D.; Mareda, J.; Matile, S. *J. Am. Chem. Soc.* **2010**, *132*, 6923–6925.

(4) Dawson, R. E.; Hennig, A.; Weimann, D. P.; Emery, D.; Ravikumar, V.; Montenegro, J.; Takeuchi, T.; Gabutti, S.; Mayor, M.; Mareda, J.; Schalley, C. A.; Matile, S. *Nat. Chem.* **2010**, *2*, 533–538.

(5) Misek, J.; Vargas Jentzsch, A.; Sakurai, S.; Emery, D.; Mareda, J.; Matile, S. *Angew. Chem., Int. Ed.* **2010**, *49*, 7680–7683.

(6) Takeuchi, T.; Matile, S. *J. Am. Chem. Soc.* **2009**, *131*, 18048–18049.

(7) Takeuchi, T.; Montenegro, J.; Hennig, A.; Matile, S. *Chem. Sci.* **2011**, *2*, 303–307.

(8) Bhosale, R.; Míšek, J.; Sakai, N.; Matile, S. *Chem. Soc. Rev.* **2010**, *39*, 138–149.

(9) Würthner, F.; Meerholz, K. *Chem.—Eur. J.* **2010**, *16*, 9366–9373.

(10) Wasielewski, M. R. *Acc. Chem. Res.* **2009**, *42*, 1910–1921.

(11) Bassani, D. M.; Jonusauskaite, L.; Lavie-Cambot, A.; McClenaghan, N. D.; Pozzo, J.-L.; Ray, D.; Vives, G. *Coord. Chem. Rev.* **2010**, *254*, 2429–2445.

(12) Thompson, B. C.; Fréchet, J. M. J. *Angew. Chem., Int. Ed.* **2008**, *47*, 58–77.

(13) Bhosale, S.; Sisson, A. L.; Talukdar, P.; Fürstenberg, A.; Banerji, N.; Vauthey, E.; Bollot, G.; Mareda, J.; Röger, C.; Würthner, F.; Sakai, N.; Matile, S. *Science* **2006**, *313*, 84–86.

(14) Perez-Velasco, A.; Gorteau, V.; Matile, S. *Angew. Chem., Int. Ed.* **2008**, *47*, 921–923.

(15) Wang, M.; Chamberland, N.; Breau, L.; Moser, J.-E.; Humphry-Baker, R.; Marsan, B.; Zakeeruddin, S. M.; Grätzel, M. *Nat. Chem.* **2010**, *2*, 385–389.

(16) Davis, J. T.; Okunola, O.; Quesada, R. *Chem. Soc. Rev.* **2010**, *39*, 3843–3862.

(17) Davis, A. P.; Sheppard, D. N.; Smith, B. D. *Chem. Soc. Rev.* **2007**, *36*, 348–357.

(18) Gale, P. A. *Acc. Chem. Res.* **2011**, *44*, 216–226.

(19) Matile, S.; Vargas Jentzsch, A.; Fin, A.; Montenegro, J. *Chem. Soc. Rev.*, DOI: 10.1039/C0CS00209G.

(20) Sakai, N.; Mareda, J.; Matile, S. *Acc. Chem. Res.* **2008**, *41*, 1354–1365.

(21) Talukdar, P.; Bollot, G.; Mareda, J.; Sakai, N.; Matile, S. *Chem.—Eur. J.* **2005**, *11*, 6525–6532.

(22) Sakai, N.; Matile, S. *J. Am. Chem. Soc.* **2002**, *124*, 1184–1185.

(23) Sakai, N.; Matile, S. *Chem.—Eur. J.* **2000**, *6*, 1731–1737.

(24) Robert, F.; Winum, J.-Y.; Sakai, N.; Gerard, D.; Matile, S. *Org. Lett.* **2000**, *2*, 37–39.

(25) Winum, J.-Y.; Matile, S. *J. Am. Chem. Soc.* **1999**, *121*, 7961–7962.

(26) Sakai, N.; Kamikawa, Y.; Nishii, M.; Matsuoka, T.; Kato, T.; Matile, S. *J. Am. Chem. Soc.* **2006**, *128*, 2218–2219.

(27) Hennig, A.; Fischer, L.; Guichard, G.; Matile, S. *J. Am. Chem. Soc.* **2009**, *131*, 16889–16895.

(28) Sakai, N.; Baumeister, B.; Matile, S. *ChemBioChem* **2000**, *1*, 123–125.

(29) Das, G.; Talukdar, P.; Matile, S. *Science* **2002**, *298*, 1600–1602.

(30) Sordé, N.; Das, G.; Matile, S. *Proc. Natl. Acad. Sci. U.S.A.* **2003**, *100*, 11964–11969.

(31) Litvinchuk, S.; Sordé, N.; Matile, S. *J. Am. Chem. Soc.* **2005**, *127*, 9316–9317.

(32) Litvinchuk, S.; Tanaka, H.; Miyatake, T.; Pasini, D.; Tanaka, T.; Bollot, G.; Mareda, J.; Matile, S. *Nat. Mater.* **2007**, *6*, 576–580.

(33) Hagihara, S.; Tanaka, H.; Matile, S. *J. Am. Chem. Soc.* **2008**, *130*, 5656–5657.

(34) Sakai, N.; Sordé, N.; Matile, S. *J. Am. Chem. Soc.* **2003**, *125*, 7776–7777.

(35) Sakai, N.; Sordé, N.; Das, G.; Perrottet, P.; Gerard, D.; Matile, S. *Org. Biomol. Chem.* **2003**, *1*, 1226–123.

(36) Ni, C.; Matile, S. *Chem. Commun.* **1998**, *33*, 755–756.

(37) Mareda, J.; Matile, S. *Chem.—Eur. J.* **2009**, *15*, 28–37.

(38) Matile, S.; Tanaka, H.; Litvinchuk, S. *Top. Curr. Chem.* **2007**, *277*, 219–250.

(39) Snaith, H. J.; Whiting, G. L.; Sun, B.; Greenham, N. C.; Huck, W. T. S.; Friend, R. H. *Nano Lett.* **2005**, *5*, 1653–1657.

(40) Foster, S.; Finlayson, C. E.; Keivanidis, P. E.; Huang, Y.-S.; Hwang, I.; Friend, R. H.; Otten, M. B. J.; Lu, L.-P.; Schwartz, E.; Nolte, R. J. M.; Rowan, A. E. *Macromolecules* **2009**, *42*, 2023–2030.

(41) Mwaura, J. K.; Pinto, M. R.; Witker, D.; Ananthakrishnan, N.; Schanze, K. S.; Reynolds, J. R. *Langmuir* **2005**, *21*, 10119–10126.

(42) Decher, G. *Science* **1997**, *277*, 1232–1237.

(43) Sakai, N.; Sisson, A. L.; Bürgi, T.; Matile, S. *J. Am. Chem. Soc.* **2007**, *129*, 15758–15759.

(44) Sisson, A. L.; Sakai, N.; Banerji, N.; Fürstenberg, A.; Vauthey, E.; Matile, S. *Angew. Chem., Int. Ed.* **2008**, *47*, 3727–3729.

(45) Bhosale, S. V.; Jani, C. H.; Langford, S. J. *Chem. Soc. Rev.* **2008**, *37*, 331–342.

(46) Sakai, N.; Mareda, J.; Vauthey, E.; Matile, S. *Chem. Commun.* **2010**, *46*, 4225–423.

(47) Thalacker, C.; Röger, C.; Würthner, F. *J. Org. Chem.* **2006**, *71*, 8098–8105.

(48) Marquardt, C. W.; Grunder, S.; Błaszczyk, A.; Dehm, S.; Hennrich, F.; von Löhneysen, H.; Mayor, M.; Krupke, R. *Nat. Nanotechnol.* **2010**, *5*, 863–867.
(49) Chopin, S.; Chaignon, F.; Blart, E.; Odobel, F. *J. Mater. Chem.* **2007**, *17*, 4139–4146.
(50) Yang, F.; Shtein, M.; Forrest, S. *Nat. Mater.* **2005**, *4*, 37–41.
(51) Lista, M.; Sakai, N.; Kel, O.; Areephong, J.; Sakurai, S.; Emery, D.; Mareda, J.; Vauthey, E.; Matile, S. To be submitted for publication.
(52) Corbett, P. T.; Leclaire, J.; Vial, L.; West, K. R.; Wietor, J.-L.; Sanders, J. K. M.; Otto, S. *Chem. Rev.* **2006**, *106*, 3652–3711.
(53) Ramström, O.; Lehn, J.-M. *Nat. Rev. Drug Discovery* **2002**, *1*, 26–36.
(54) Schottel, B. L.; Chifotides, H. T.; Dunbar, K. R. *Chem. Soc. Rev.* **2008**, *37*, 68–83.
(55) Gamez, P.; Mooibroek, T. J.; Teat, S. J.; Reedijk, J. *Acc. Chem. Res.* **2007**, *40*, 435–444.
(56) Estarellas, C.; Frontera, A.; Quiñonero, D.; Deyà, P. M. *Angew. Chem., Int. Ed.* **2011**, *50*, 415–418.
(57) Cavallo, G.; Metrangolo, P.; Pilati, T.; Resnati, G.; Sansotera, M.; Terraneo, G. *Chem. Soc. Rev.* **2010**, *39*, 3772–3783.
(58) Takeuchi, T.; Sakai, N.; Matile, S. *Faraday Discuss.* **2009**, *143*, 187–203.
(59) Butterfield, S. M.; Miyatake, T.; Matile, S. *Angew. Chem.* **2009**, *121*, 331–334.
(60) Lavigne, J. J.; Anslyn, E. V. *Angew. Chem., Int. Ed.* **2001**, *40*, 3118–3130.
(61) Suslick, B. A.; Feng, L.; Suslick, K. S. *Anal. Chem.* **2010**, *82*, 2067–2073.
(62) Palacios, M. A.; Nishiyabu, R.; Marquez, M.; Anzenbacher, P., Jr. *J. Am. Chem. Soc.* **2007**, *129*, 7538–7544.
(63) Montenegro, J.; Matile, S. *Chem.—Asian J.* **2011**, *2*, 281–289.
(64) Montenegro, J.; Bonvin, P.; Takeuchi, T.; Matile, S. *Chem.—Eur. J.* **2010**, *16*, 14159–14166.
(65) Montenegro, J.; Fin, A.; Matile, S. *Org. Biomol. Chem.* **2011**, *9*, 2641–2647.
(66) Sakai, N.; Matile, S. *J. Am. Chem. Soc.* **2003**, *125*, 14348–14356.
(67) Rothbard, J. B.; Jessop, T. C.; Lewis, R. S.; Murray, B. A.; Wender, P. A. *J. Am. Chem. Soc.* **2004**, *126*, 9506–9507.
(68) Takeuchi, T.; Kosuge, M.; Tadokoro, A.; Sugiura, Y.; Nishi, M.; Kawata, M.; Sakai, N.; Matile, S.; Futaki, S. *ACS Chem. Biol.* **2006**, *1*, 299–303.
(69) Woolfson, D. N.; Mahmoud, Z. N. *Chem. Soc. Rev.* **2010**, *39*, 3464–3479.
(70) Whitesides, G. M.; Deutch, J. *Nature* **2011**, *469*, 21–22.